Scientific paper

Kinetically Governed Formation of $d(G_4T_2G_4)$ Assemblies

Iztok Prislan, Andrej Jamnik and Matija Tomšič*

University of Ljubljana, Faculty of Chemistry and Chemical Technology, Aškerčeva 5, SI-1000 Ljubljana, Slovenia

** Corresponding author: E-mail: Matija.Tomsic@fkkt.uni-lj.si*

Received: 27-02-2012

Dedicated to Prof. Dr. Gorazd Vesnaver on the occasion of his 70th birthday

Abstract

The most frequently appearing form of DNA is a double helical structure in which two single strands are held together by Watson-Crick base pairs. In addition, guanine rich DNA sequences are known to adopt several unusual structures with G-quartet as a basic repeating motif. Recently large self-assembling nanostructures, called G-wires have become of great interest because of their potential use in molecular electronics. To better understand the forces driving structural transitions of G-wires formed from $d(G_4T_2G_4)$ oligonucleotide in Na^+ solutions, we employed a number of techniques such as UV and CD spectroscopy, differential scanning calorimetry (DSC), gel electrophoresis, small angle X-ray scattering (SAXS) and dynamic light scattering (DLS). All the experimental techniques showed that thermally induced folding transitions depend on the cooling rate. In addition, DSC shows that thermally induced unfolding transition depends on heating rate, thus leading to the conclusion that structural transitions of $d(G_4T_2G_4)$ are kinetically governed processes.

Keywords: DSC, CD, SAXS, DLS, G-quadruplex, G-wires

1. Introduction

It seems that unusual structures of RNA and DNA have not yet revealed all of their secrets. Guanine rich DNA sequences have been of particular interest since their presence is supposed to be crucial to a number of important biological processes. For instance telomeres at the end of chromosomes contain repeats of nucleotides that are guanine rich and may form G-quadruplexes.[1,2] Formation of telomeric G-quadruplexes inhibits the activity of enzyme telomerase required for the uncontrolled growth of majority of cancer cells.[3–9] Proliferation of various cancer cells can also be achieved with specific quadruplex-forming oligonucleotide aptamers that are able to bind to certain cellular proteins.[10,11] G-quadruplex forming oligonucleotides can also act as antiviral agents,[12,13] potassium sensing agents[14] or can influence control regions of some oncogenes.[15,16]

G-quadruplex structures consist of stacked G-quartets formed by a cyclic coplanar Hoogsteen base pairing of the four participating guanines.[17,18] The pairing of guanines and stacking of G-quartets is very versatile.[19] G-quadruplexes are renowned for their structural diversity with the strand polarity and glycosidic torsion angles strongly dependent on the nature of the cations, the connecting loops, and the capping bases.[20–22] G-quadruplexes are usually formed from one (monomolecular), two (bimolecular) and four (tetramolecular) single strands, but some of the guanine rich oligonucleotides can create large self-assembling nanostructures like G-wires[23] as shown in Figure 1, Frayed-wires[24] or G-lego.[25] These structures are of growing interest because oxidation potential of guanine is the lowest among deoxynucleotide bases. These guanine rich sequences may act as functional elements in molecular electronics.[26]

These superstructures represent a challenge also in terms of basic understanding of forces that drive their formation. The problem is that our understanding of G-quadruplex formation and structure is rather limited even for short sequences comprising only 3–4 G-quartets.[27] This is mainly due to the presence of multiple conformations in solution that may undergo kinetically governed interconversions and folding/unfolding transitions. Recently our lab has investigated polymorphism of quadruplexes formed from $d(G_4T_4G_3)$ in Na^+ and K^+ solutions.[28,29] We have confirmed that the formation and unfolding of certain G-quadruplexes are kinetically governed processes. In the present work the thermally induced structural transitions of supermolecular assemblies using a simple 10 nucleotide sequence $d(G_4T_2G_4)$ in Na^+ solutions was followed to test a wider

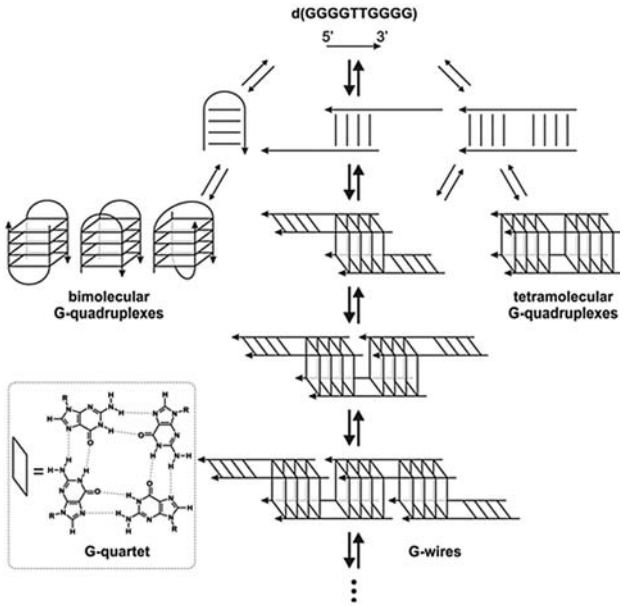

Figure 1: Comparison of G-quadruplex conformations that $d(G_4T_2G_4)$ oligonucleotide may adopt as represented by Marsh et al.[30]

applicability of such approach. Furthermore, we interpret the transitions in terms of a kinetically governed coexistence of several quadruplex structures and the unfolded single strand form. To reach this goal we employ a number of techniques such as UV and CD spectroscopy, gel electrophoresis, small angle X-ray scattering (SAXS), dynamic light scattering (DLS), and differential scanning calorimetry (DSC). The first three experimental techniques, along with atomic force microscopy (AFM) have already been engaged to characterize G-wires formed by telomeric DNA repeat $d(G_4T_2G_4)$.[30] Similarly, SAXS and DLS have already been used successfully to study overall molecular shape and aggregate size of G-quadruplexes,[31–33] but their usage is still very scarce in such studies. In this work we will demonstrate the applicability of SAXS and DLS in determination of structural features of G-quadruplex structures.

2. Experimental and Methods

2. 1. Materials

The $d(G_4T_2G_4)$ oligonucleotide was obtained HPLC pure from Midland Co. U.S.A. DNA was first dissolved in water and then extensively dialyzed against the buffer (three changes of buffer solutions in 24 h) using a dialysis tube Float-A-Lyser (Spectrum Laboratories, USA, Mw cutoff 500 Da). Its concentrations in buffer solutions were determined spectrophotometrically at 25 °C. The value of $\varepsilon_{260} = 99000\ M^{-1}\ cm^{-1}$, which was estimated from the nearest-neighbor data of Cantor et al.,[34] was used for the extinction coefficient of oligonucleotide's single stranded form at 25 °C. The buffer used in all experiments consisted of 20 mM Na-cacodylic buffer, 1 mM EDTA and 30 mM NaCl (pH = 6.9). Initially all the samples were transformed into single-stranded form by heating in an outer thermostat at 95 °C for 5 min, cooled down to 4 °C at the cooling rates of 0.05 or 1.0 °C/min to form quadruplex structures and then used in the UV, CD, DLS, SAXS, DSC and PAGE experiments.

2. 2. UV Melting Experiments

Absorbance versus temperature profiles of $d(G_4T_2G_4)$ samples were measured in 0.25 mm path-length cells using a Cary 100 BIO UV/Visible Spectrophotometer (Varian Inc.) equipped with a thermoelectric temperature controller. Thermally induced folding/unfolding transitions of $d(G_4T_2G_4)$ quadruplex samples ($c \approx 1.1$ mM in single strands) prepared either at the cooling rate of 0.05 or 1.0 °C/min were monitored between 5 and 95 °C at λ = 295 nm at the heating/cooling rate of 1.0 °C/min.

2. 3. CD Spectroscopy

CD spectra of $d(G_4T_2G_4)$ quadruplexes in Na^+ solutions were measured as a function of temperature in an AVIV CD Spectropolarimeter 62A DS, equipped with a thermoelectric temperature controller. Ellipticity, θ, was measured between 5 and 95 °C in the temperature intervals of 3 °C at the average heating rate of 1.0 °C/min. CD spectra of samples ($c \approx 1.1$ mM in single strands) prepared at either of the cooling rates, corrected for the corresponding buffer contribution, were collected between 220 and 320 nm in a 0.25 mm cuvette at 60 nm/min, signal averaging time of 2 s and 5 nm bandwidth. Molar ellipticity, $[\theta]$, was obtained from equation $[\theta] = \theta/(c \cdot l)$, where l stands for the path-length through the cuvette. In all experiments a 0.25 mm quartz glass cuvette was used.

2. 4. Differential Scanning Calorimetry (DSC)

DSC experiments were performed using a Nano DSC II instrument (Calorimetry Sciences Corp., UT, USA) on the samples that were previously prepared by temperature treatment in an outer thermostat (cooling rate of 0.05 or 1.0 °C/min and a subsequent annealing at 4 °C). Quadruplex concentration used in these DSC studies was 1.1 mM in single strands. Cyclic DSC measurements were performed at the heating rates of 0.5, 1.0 and 2.0 °C/min and a single cooling rate of 1.0 °C/min. Therefore the effect of different sample preparation (temperature treatment) in an outer thermostat was only observed during the first DSC melting scan. From there on the temperature treatment in the DSC apparatus was equal for all the samples (same sequence of heating rates and the same cooling rate of 1.0 °C/min). The measured temperature interval was between 4 °C and 95 °C. The corresponding baseline (buffer-buffer) scans were

subtracted from the unfolding/folding scans (i.e. heating/cooling scans) prior to their normalization and analysis. The total enthalpy of unfolding or folding, ΔH_{tot}, was obtained from the measured DSC thermograms as the area under the $\Delta C_P = \overline{C}_{P,2} - \overline{C}_{P,S}$ versus T curve, where $\overline{C}_{P,2}$ is the measured partial molar heat capacity corrected for the baseline and normalized to 1 mole of quadruplex in single strands, and $\overline{C}_{P,S}$ is the corresponding partial molar heat capacity of the unfolded single stranded state obtained by extrapolation from high temperatures over the whole measured temperature interval.

2. 5. Gel Electrophoresis

G-quadruplex structures formed upon cooling of single-stranded DNA ($c \approx 340$ μM in 20 mM Na-cacodylic buffer, 1 mM EDTA and 30 mM NaCl) at the cooling rate of 0.05 or 1.0 °C/min were studied by non-denaturing PAGE performed on 20% polyacrylamide gels supplemented with 50 mM NaCl. G-quadruplex samples prepared at either of the cooling rates were loaded on gels and the electrophoreses were run at 20 °C (3.5 h), at 10 V/cm (I = 300 mA). Bands in the gel were followed by UV shadowing at $\lambda = 254$ nm without any markers. Afterwards gel was submerged in small volume of 0.5 μg/ml EtBr. Gel was allowed to stain for 10 minutes at room temperature and after destaining in H_2O placed on a transilluminator. Bands were photographed at excitation wavelength of 302 nm. To facilitate comparisons between the bands observed with different samples the double stranded $d(G_4T_4G_4)_2$ quadruplex and $d(GA_5C_5T_5C)$ hairpin were used as control oligonucleotides.

2. 6. Small-Angle X-Ray Scattering Measurements

Small-angle X-ray scattering (SAXS) spectra were measured with a modified version of the Kratky compact camera (Anton Paar KG, Graz, Austria).[35] The camera was attached to a conventional X-ray generator Krislalloflex 760 (Bruker AXS GmbH, Karlsruhe, Germany) that was operating at 40 kV and 35 mA. As a source of X-rays the sealed X-ray tube with a cooper anode was used. Utilizing the modern focusing multilayer optics (Max Flux#) the Cu K_α X-rays with a wavelength $\lambda = 0.154$ nm were filtered out. In addition a software monochromator was also used, which considered only the scattered X-ray photons within a predefined window of energies and in this way eliminated also possible remaining hard X-rays from the detected scattered light. The samples were measured in a standard quartz capillary with an outer diameter of 1 mm and wall thickness of 10 μm. The scattered X-ray intensities were detected with the position sensitive detector PSD ASA (M. Braun GmbH, Garching, Germany) in the small-angle regime of scattering vectors $0.07 < q < 7$ nm^{-1}, where $q = 4\pi/\lambda \cdot \sin(\vartheta/2)$, ϑ being the scattering angle. The measuring times of 20 hours yielded satisfactory measuring statistic. Scattering data were corrected for the empty capillary and solvent scattering and put on absolute scale using water as a secondary standard.[36] However, the SAXS intensities obtained in this way were still experimentally smeared due to finite dimensions of the primary X-ray beam;[37] therefore the experimental scattering intensities were desmeared simultaneously during the evaluation procedure.

2. 7. Dynamic Light Scattering Measurements

Dynamic light scattering (DLS) measurements were performed on a 3D-DLS Spectrometer (LS Instruments, Switzerland). The instrument was equipped with a 35 mW He-Ne laser ($\lambda = 632.8$ nm), high precision beam-splitter, focusing entrance and collimating exit lens and two single-mode fiber-optics detectors with avalanche photodiodes (photo detection efficiency > 65 %). Samples were measured in the scattering cells that were immersed in a large-diameter thermostated bath of index matching liquid (decaline). Utilizing the primary-beam attenuator the counting rates were adjusted to about 500 kHz at an angle of 90° to the direction of the primary beam. The instrument was used in a 3D-cross-correlation scheme. A number of DLS measurements of 2 minutes each for nonfiltered samples and 30 minutes each for the filtered sample (filtered through the filter with pore-size of 20 nm; Whatman Anotop® 25 Plus – syringe filters containing proprietary alumina based Anopore membrane with glass microfiber prefilter were used) were collected and approximately 15 of them were averaged to obtain the final autocorrelation function. All the measurements were performed at an angle of 90° to the direction of the primary beam.

2. 8. Indirect Fourier Transformation of SAXS Data

For detailed analysis of experimental SAXS curves the Generalized Indirect Fourier Transformation GIFT[38–43] software package was used. However, solely the use of its basic part, i.e. the Indirect Fourier Transformation method IFT,[44–46] was sufficient in our case, because there were no considerable effects of interparticle interactions on the scattering data observed for the studied samples. IFT is namely a completely model-free method, which is appropriate only for dilute particulate systems with negligible interparticle interactions. It is based on the fact that the form factor, $P(q)$, which represents the intraparticle scattering contribution, can be written as the Fourier transformation of the pair-distance distribution function $p(r)$:[44,45]

$$P(q) = 4\pi \int_0^\infty p(r) \cdot \frac{\sin(qr)}{qr} \cdot dr \,, \qquad (1)$$

where r is the distance between two scattering centers within the particle. Pair-distance distribution function serves as a tool for the determination of the scattering particles' geometry.[42,47] At distances r bigger than the maximum dimension of particle the $p(r)$ function adopts the value of zero and in this way provides a useful tool for determination of the particle's maximum dimension. Furthermore, from the shape of this function the type of scattering particles' symmetry can be deduced.[47]

2. 9. Evaluation of Dynamic Light Scattering Results

During dynamic light scattering experiments the fluctuations of the scattering intensity are monitored. These fluctuations are directly related to the fluctuations of the scattering amplitudes, which originate from the concentration fluctuations arising from Brownian movement[48,49] of the scattering particles in solution. The fluctuations of the scattering amplitude can be expressed in a form of the scattering amplitude (field) autocorrelation function $G_1(\tau)$, which is connected to the diffusion coefficient of free scattering particles D_o with the following relation:[50,51]

$$G_1(\tau) = e^{-D_o q^2 \tau}, \quad (2)$$

where τ is the delay time and $q = (4\pi n_s/\lambda_o) \sin(\vartheta/2)$, with n_s being the refractive index of the solvent and λ_o the wavelength of the light in vacuum. Unfortunately, it is experimentally not possible to obtain $G_1(\tau)$ directly. The raw result of DLS experiment is namely a time-dependent intensity autocorrelation function $G_2(\tau)$, which is connected to $G_1(\tau)$ by the Siegert equation:[52]

$$G_2(\tau) = B + C\left[G_1(\tau)\right]^2, \quad (3)$$

where parameter B is the baseline and constant C represents the strength of the coherent signal. The DLS method is in majority of cases used for particle sizing. In this manner it exploits the well-known Stokes-Einstein equation, which provides the connection between the diffusion coefficient of globular scattering particles D_o and the hydrodynamic radius R_H:

$$R_H = \frac{k_B T}{6\pi\eta D_o}, \quad (4)$$

where k_B is the Boltzmann constant, T is the temperature, and η the dynamic viscosity of the solvent. DLS technique is therefore a useful tool for determination of the hydrodynamic radii of the scattering particles. However, one has to be aware that the hydrodynamic radius is by definition the radius of a hypothetical spherical particle that would have the same diffusion coefficient as the scattering particles do have in the studied sample (solvent). This means that R_H is a parameter determined exclusively on the basis of dynamic properties of the scattering particles that are influenced also by the interparticle interactions; i.e. the scattering particles actual shape and size has only an indirect influence on the R_H.

In the case of polydisperse systems the field autocorrelation function $G_1(\tau)$ is represented by an integral over many exponentials:

$$G_1(\tau) = \int_{\tau_{min}}^{\tau_{max}} D(\tau_c)\ W(\tau_c)\ e^{-\frac{\tau}{\tau_c}}\ \frac{1}{\tau_c^2}\, d\tau_c, \quad (5)$$

where τ_c is the relaxation time defined as $\tau_c = 1/D_0 q^2$, the function $D(\tau_c)$ represents the continuous distribution of relaxation times τ_c, and $W(\tau_c)$ a corresponding weighting function depending on the kind of distribution (number, volume or intensity distribution) adopting the value of τ_c^6, τ_c^3 or 1, respectively. Combination of Equation (3) and Equation (5) allows the determination of $D(\tau_c)$ from the experimentally determined $G_2(\tau)$ function. $D(\tau_c)$ can easily be converted into the more commonly used distribution function of hydrodynamic radii $D(R_H)$.[53] Expression described by Equation (5) is a modified Laplace transformation. The distribution functions presented later in this paper were obtained by inverse Laplace transformation of experimental data utilizing the program ORT (Optimized Regularization Technique).[53]

3. Results and Discussion

3. 1. Thermaly Induced Folding and Unfolding of d($G_4T_2G_4$) Quadruplexes

It has already been observed previously that formation and unfolding of certain sequences of G-quadruplexes are governed kinetically. In order to test whether that applies also to d($G_4T_2G_4$) quadruplexes we have first recorded a series of UV heating/annealing curves. The results of such experiments are shown in Figure 2. The dashed line corresponds to the melting curve, which was recorded for the sample that was previously heated up to 95 °C and then slowly (0.05 °C/min) cooled down to 5 °C in an outer thermostat. The shape of this curve suggests that unfolding of d($G_4T_2G_4$) quadruplexes is a biphasic transition. The estimated melting temperatures, T_M s, are 54 and 87 °C for the first and second transition, respectively. An annealing curve during the cooling cycle with the rate of 1 °C/min was recorded next (see dotted line in Figure 2). This curve suggests that folding of our quadruplex is a monophasic transition with T_M of about 51 °C. Immediately after such cooling cycle the UV melting curve was recorded once more (see full line in Figure 2). In contrast to the bimodal shape of the first UV melting curve its shape is typical for monophasic transition with T_M of about 53 °C. Several additional cycles consisting of melting and

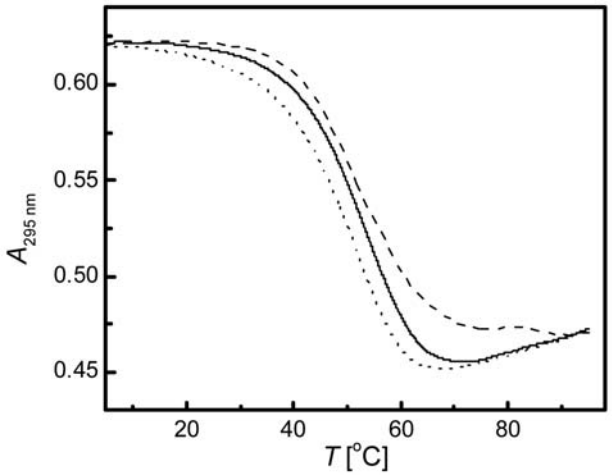

Figure 2. UV-melting and cooling curves at 295 nm for d($G_4T_2G_4$) quadruplexes in 20 mM Na-cacodylate buffer solution at pH = 6.9 and $C(Na^+)$ = 50 mM. Melting curve of quadruplex sample prepared at the cooling rate of 0.05 °C/min and measured at the heating rate of 1 °C/min (dashed line). Reproducible loops consisting of the melting curves determined at the heating rate of 1 °C/min (full line) and cooling curves observed at the cooling rate of 1 °C/min (dotted line).

annealing curves were recorded afterwards, but were all found to be reproducible. These UV absorbance measurements obtained in the presence of Na^+ ions therefore show hysteresis of the UV melting and annealing curves, which depends on the heating and cooling rate. The observed hysteresis suggests that folding/unfolding of various d($G_4T_2G_4$) structures is a kinetically governed process. Different rates of cooling resulted in changes of shape and T_M s of UV unfolding curves. This effect has already been reported by our lab[28,29] We attributed observed differences to the kinetically governed formation of more than one structure. Results presented in Figure 2 suggest that after slow cooling (0.05 °C/min) there are at least two predominant conformers whereas in the case of moderate cooling (1 °C/min) there seems to be only one conformer present in the solution.

In order to support UV results and to get some further insight on the conformation of quadruplexes occurring in solution we also measured the temperature dependence of CD spectra of two d($G_4T_2G_4$) samples prepared at the cooling rates of 0.05 and 1.0 °C/min, respectively. These results are shown in Figure 3. CD spectra of the model quadruplexes with parallel strands are characterized by a peak around λ = 264 nm and arround 240 nm, while those with antiparallel strands exhibit peaks at around 295 nm and troughs at arround 265 nm.[54–56] We expected predominant formation of G-wires and consequently our results to resemble CD spectra of model quadruplexes with parallel strands. By contrast, samples prepared at either slow or moderate cooling rate and recorded at 5 °C exhibit a negative minimum at 240 nm, a large positive band at 262 nm and another positive band at 291 nm. The origin for unexpected CD spectra may be narrowed down to two causes. First of all the shape of CD spectra of G-quadruplexes is determined by the population of syn/anti geometries of guanosine glycosidic torsion angles and this geometry is not directly related to the strand orientation. That would mean that majority of population might still adopt conformation of G-wires and the CD spectra would differ from CD spectra of model quadruplexes with parallel strands. The second explanation for our results is more straightforward. It might be possible that formation of G-wires is not a major pathway under conditions used during our experiments but is just one of the many, more or less equally probable processes leading to different conformations of G-quadruplexes as shown in Figure 1. Thus positive peaks at λ = 262 and 291 nm may indicate possible presence of mixture of parallel, antiparallel or/and hybrid type of quadruplex structures.

When samples prepared at slow cooling rate are compared to those prepared at moderate cooling rate (see Figure 3) we can see that the later have a slightly lower molar ellipticity at λ = 262 nm and slightly higher molar ellipticity at 291 nm. Such behavior suggests that the association of the d($G_4T_2G_4$) single strands into the corresponding G-quadruplexes is a kinetically governed process that, depending on the cooling rate, leads to a different composition of G-quadruplex structures formed at low temperatures. Even though CD spectroscopy can provide only indicative information on strand orientation we can speculate from the shape of the curves and the increased molar ellipticity at 262 nm that slow cooling rate favors formation of G-wires due to their apparent parallel strand orientation.

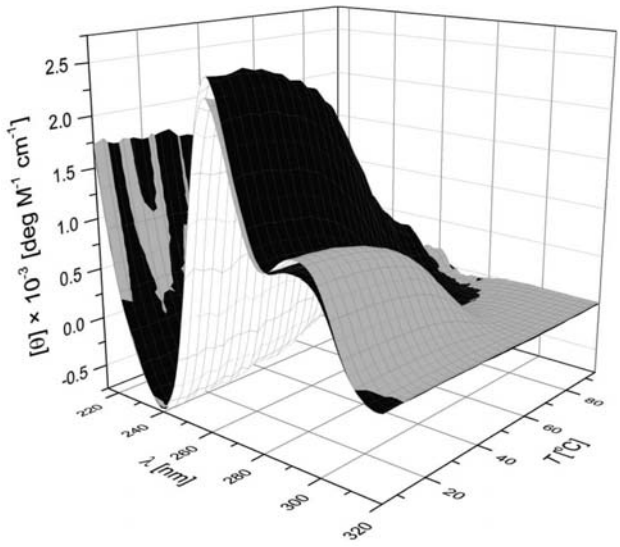

Figure 3. Temperature dependence of CD spectra of d($G_4T_2G_4$) quadruplexes in in 20 mM Na-cacodylate buffer solution at pH = 6.9 and $C(Na^+)$ = 50 mM prepared at the cooling rate of either 0.05 °C/min (black surface) or 1 °C/min (grey surface). The measured ellipticity was normalized to 1 M single strand concentration and 1 cm path length of light.

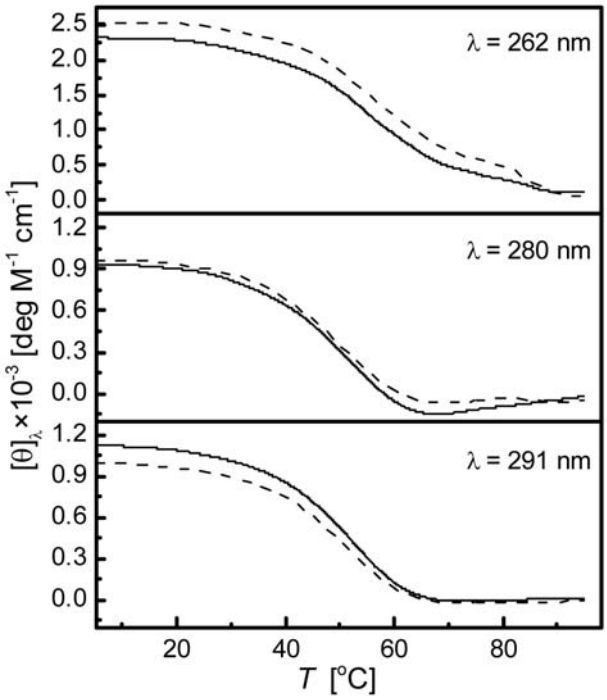

Figure 4. CD melting curves of $d(G_4T_2G_4)$ quadruplexes in 20 mM Na-cacodylate buffer solution at pH = 6.9 and $C(Na^+)$ = 50 mM prepared at the cooling rate of either 0.05 °C/min (dashed lines) or 1 °C/min (full line). The measured ellipticities at λ = 262, 280 and 291 nm were normalized to the one obtained for 1 M single strand concentration and 1 cm path length. Concentration of $d(G_4T_2G_4)$ was 1.1 mM.

The measured changes of CD peak positions and ratios of their magnitudes during unfolding reflect structural (topology) changes of the measured G-quadruplexes. In Figure 4 we show CD melting curves at wavelengths where changes in spectra are well defined, i.e. at λ = 262 and 291 nm. Melting curve obtained at λ = 262 nm for the sample prepared at slow cooling rate agrees with UV data that suggest unfolding of $d(G_4T_2G_4)$ quadruplexes in biphasic transition with T_M s of 54.5 and 85 °C for the first and second transition, respectively. The melting curve of sample prepared at moderate cooling rate also suggests biphasic transition with T_M staying approximately the same but with second transition being significantly smaller in extent. Melting curves at λ = 291 nm for the samples prepared at either cooling rate show only one transition with T_M being 51.5 °C for the sample prepared at slow cooling rate and 52.5 °C for the sample prepared at moderate cooling rate. The presence of at least two different structures would explain the obtained CD melting curves. It seems that during slow and moderate cooling $d(G_4T_2G_4)$ oligonucleotide forms G-wires, bimolecular and possibly tetramolecular G-quadruplexes. Bimolecular quadruplexes can adopt three different conformations with parallel and antiparallel strand orientation. Unfolding of these conformations is probably the cause for first transition between 51 and 55 °C and would also explain why it can be observed at both wavelengths (i.e. 262 and 291 nm). Since CD melting curve measured at λ = 291 nm did not show any transition between 70 and 95 °C, we can speculate that the transition observed at λ = 262 nm in the same temperature interval is caused by unfolding of structure with parallel strand orientation. Our guess is that transitions at higher temperatures are caused by unfolding of G-wires. They can adopt different lengths and their polydispersity in length is probably the reason why there is a steady decay observed after the first and before second transition in a CD melting curve obtained at 262 nm. At the highest measured temperatures (~ 95 °C) CD signals of all structures are lost indicating that they undergo a complete unfolding into single-stranded forms.

We have employed DSC to find out whether the measured melting processes of structures formed by $d(G_4T_4G_4)$ oligonucleotide involve one or several kinetically governed interconversions and folding/unfolding transitions. Thermograms of $d(G_4T_2G_4)$ quadruplexes measured in the presence of 50 mM NaCl at three different heating rates with the starting sample prepared at very slow or moderate rate of cooling are presented in Figure 5. They show a significant dependence on the heating and cooling rate. The most pronounced differences are observed between the DSC heating curves measured at a given heating rate for quadruplex samples prepared by the thermally induced folding at very low (0.05 °C/min)

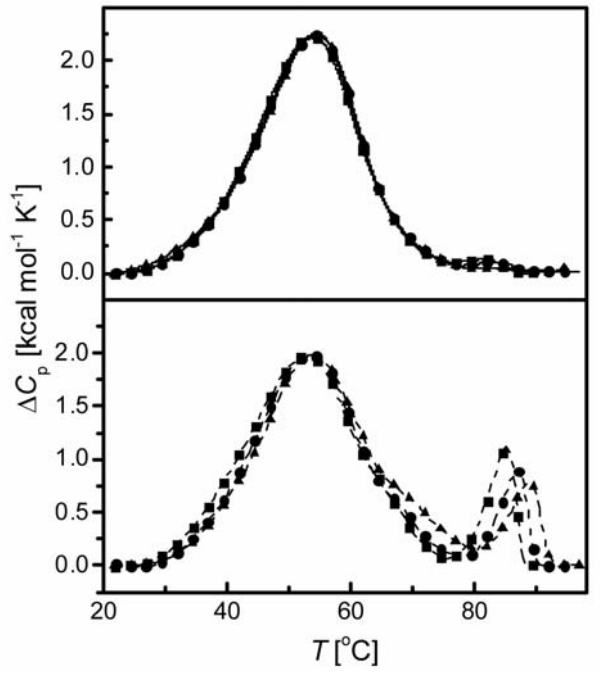

Figure 5. DSC thermograms of $d(G_4T_2G_4)$ quadruplexes in in 20 mM Na-cacodylate buffer solution at pH = 6.9 and $C(Na^+)$ = 50 mM. The ΔC_P (per mol of single strands) vs T curves measured at the heating rate of 0.5 °C/min (■), 1 °C/min (●) and 2 °C/min (▲) for quadruplex samples prepared at the cooling rate of either 0.05 °C/min (bottom) or 1.0 °C/min (top).

and moderate (1.0 °C/min) cooling rates. When samples were prepared at slow cooling of 0.05 °C/min, the DSC heating curves show at least three structural transitions (two peaks and a shoulder at 65 °C) which indicates the presence of at least three G-quadruplex structures at low temperatures. By contrast, samples prepared at moderate cooling of 1.0 °C/min are characterized by DSC melting curves that reflect at least two structural transitions (huge and small peak). For samples prepared either at the cooling rate of 0.05 or 1.0 °C/min the measured DSC heating and cooling curves were highly reproducible at all measured heating and cooling rates. The difference between samples prepared at slow and moderate cooling rates is in accordance with results obtained from spectroscopic techniques. Inspection of all DSC results shows that the total area under the measured DSC thermograms is the same (within few %) regardless of the cooling rate at which the samples were prepared and regardless of the heating rate at which they were unfolded (see Figure 5). The overall enthalpy of unfolding, ΔH_{tot}, equals 25 kcal per mole of oligonucleotide and approximately 3 kcal per mole of guanine. Let's assume that all of the guanines are involved in G-quadrupleks formation. Since G-quartets consist of four guanines we can conclude that the average enthalpy of G-quadruplexs unfolding expressed per mole of G-quartets equals 12 kcal/mol. This value is somewhat lower than the corresponding literature data (between 15 and 20 kcal/ mol), and suggests the existence of unpaired guanines.

Even though the top panel of Figure 5 shows that unfolding of $d(G_4T_2G_4)$ does not depend on heating rate, the bottom panel tells a very different story. The last peak in DSC melting thermograms of $d(G_4T_2G_4)$ prepared at very slow cooling rate shifts with increasing heating rate (0.5 → 1.0 → 2.0 °C/min) to higher temperatures (85 → 87 → 89 °C). This shifts can also be considered as indication of kinetically governed folding and unfolding transitions of structures formed by $d(G_4T_2G_4)$.

3. 2. Structural Characterization of $d(G_4T_2G_4)$ Quadruplexes

In line with the conclusions based on the described CD and DSC measurements, also gel migration experiments revealed a coexistence of three groups of migrating structural forms as depicted in Figure 6. The fastest migrating group consists of two major bands. The slowest of these two bands travels with approximately the same speed as $d(G_4T_4G_4)_2$ control oligonucleotide. We believe that because of the similar size (24 vs. 20 nucleotides) the bands in fastest migrating group correspond to possible conformations of bimolecular structure of $d(G_4T_2G_4)_2$. Two different bands clearly point to the presence of at least two different bimolecular conformers which agrees nicely with conclusions based on the CD melting curves. The middle group consists of three major bands. Based on the position of bimolecular quadruplexes and the possible structures $d(G_4T_2G_4)$ oligonucleotide can adopt we speculate that these bands originate from the next simplest highly ordered structure, that is, tetramolecular structure of $d(G_4T_2G_4)_4$. The three bands may represent the first two states appearing in the formation of G-wires and the tetra-

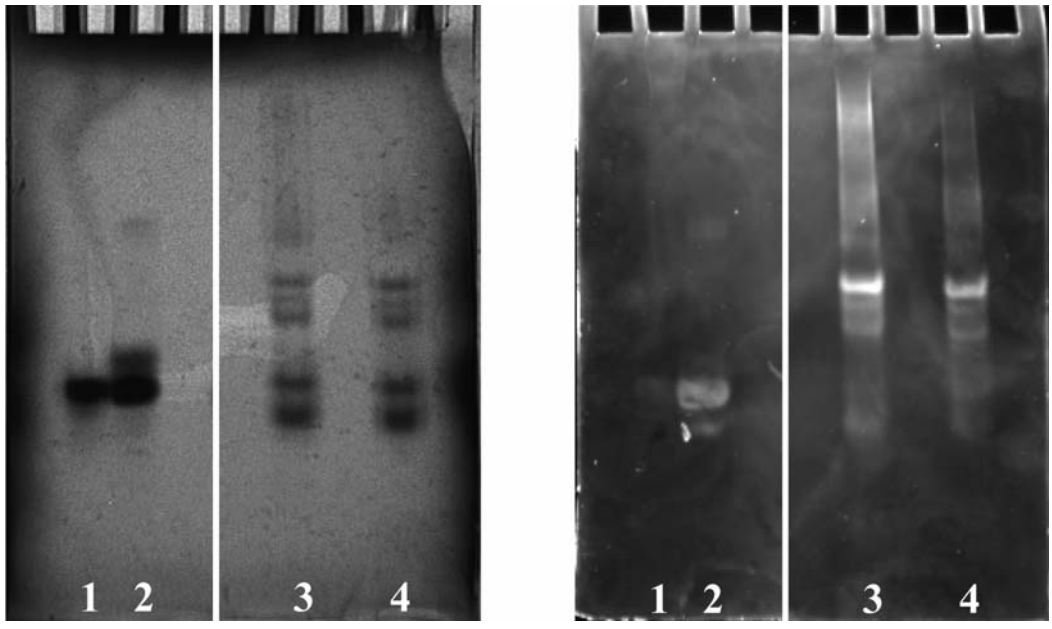

Figure 6. Non denaturing PAGE (20 %) of $d(G_4T_2G_4)$ quadruplexes prepared at the cooling rate of either 0.05 °C/min (3) or 1 °C/min (4). a) Bands were followed by UV shadowing (λ = 254 nm) at the constant temperature of 20 °C. As control oligonucleotide double stranded $d(G_4T_4G_4)_2$ quadruplex marker (1) and $d(GA_5C_5T_5C)$ hairpin marker (2) were used. b) The same gel was stained with EtBr and bands were followed by transilluminator at λ = 302 nm.

molecular G-quadruplex (see Figure 1). The third group of slowly migrating structures looks like one long, smeared band which stretches from the beginning of the gel and up to the beginning of the second group of bands. It most likely consists of multiple structures with different sizes which originate from different stages of G-wire formation. The presence of G-wires with different sizes is in accordance with literature[30,57] and also agrees with our CD-melting curves and DSC thermograms. The contents of these groups seem to depend on the cooling rate at which the samples are prepared. The gel experiments show that samples prepared at the cooling rate of 0.05 °C/min are characterized by a more pronounced slowest migrating group thus indicating that a higher proportion of the G-wires is very likely responsible for the second transition observed in UV and CD melting curves. Higher percentage of G-wires may also be responsible for the appearance of second peak at about 85 °C in DSC thermograms. Since this peak shifts to higher temperatures with increasing heating rate we can speculate that formation of G-wires is kinetically governed process. On the other hand, the samples prepared at a moderate cooling rate of 1.0 °C/min are characterized by a more pronounced fastest migrating group resulting from higher portion of bimolecular quadruplexes compared to G-wires. The negligible intensity of slowest migrating group of samples prepared at either slow or moderate cooling rate along with the enthalpies obtained from DSC data suggest that even though the structures of different lengths are present in solution, $d(G_4T_2G_4)$ folds predominately into shorter G-wires.

The same gel was stained with EtBr and resulting bands are shown in Figure 6b. As expected, EtBr does not bind to $d(G_4T_4G_4)_2$ control oligonucleotide, therefore no bands can be visible in the first lane. On the other hand, EtBr interacts with the second control oligonucleotide which is in accordance with other control oligonucleotides that form hairpin structures. The fastest migrating group of our sample seems to interact with EtBr with negligible affinity. This is in accordance with our suggestion that this group probably consists of bimolecular quadruplexes which have a very low binding affinity to EtBr. The middle migrating group is comprised of structures which according to the intensity of bands exhibit stronger interaction with EtBr. The slowest band in this group shows as a strongest single band on the stained gel. The slowest migrating group also exhibits stronger interaction with EtBr when compared to bimolecular quadruplexes suggesting that EtBr binds to G-wires with significant affinity.

These findings were further supported by the DLS measurements presented in Figure 7, which were obtained for the sample with quadruplexes prepared at the cooling rate of 0.05 °C/min (slow cooling) and the cooling rate of 1 °C/min (fast cooling). In Figure 7a the corresponding intensity autocorrelation functions are depicted. Already these raw DLS results reveal the bimodal shape of $G_2(\tau)$ function which clearly indicate the presence of two populations with very different dynamic properties in the sample, i.e. "bigger-particle" and "smaller-particle" population. In addition the slowly cooled sample was filtered through a filter with pore-size of 20 nm in order to isolate the smaller-particle population and analyze it independently. The obtained monomodal form of $G_2(\tau)$ function in this case confirms that by filtration only the smaller-particle population was successfully separated out. In the next step all these raw data were further analyzed performing indirect inverse Laplace transformation utilizing the ORT technique.[53] The corresponding results are presented in Figure 7b in a form of intensity weighted distribution of hydrodynamic radii $D(R_H)$. To facilitate the mutual comparison of these results, the distributions obtained for slowly and fast cooled sample are normalized to the height of the peak of the population of bigger-particle population. In addition, the filtered sample is also normalized to the height of the peak of the small-particle population for slowly cooled sample. At this point we have to

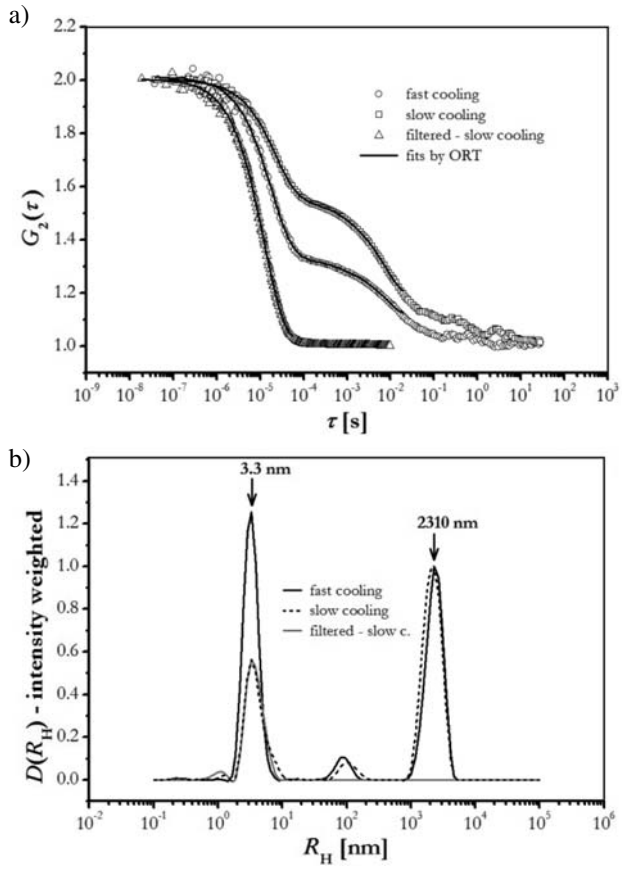

Figure 7. Dynamic light scattering results for the sample with quadruplexes prepared at the cooling rate of either 0.05 °C/min (slow cooling) or the cooling rate of 1 °C/min (fast cooling) all measured at an angle of 90° to the direction of the primary beam. The former sample was also filtered through the filter with pore-size of 20 nm. (a) Experimental DLS intensity autocorrelation function $G_2(\tau)$ (symbols) with the corresponding fits according to the ORT evaluation (lines). (b) Inverse Laplace transformation of the DLS results: scattering intensity weighted distribution function $D(R_H)$.

stress that the obtained values of the hydrodynamic radii are quantitatively valid only for the small-particle population showing the average effective sizes around 3.3 nm. Namely, at higher values of R_H the DLS results are expected to be dependent on the scattering angle of the measurement, but we have not explored such dependence in our experiments. Such dependence is expected since the size of these particles is already comparable or larger to the size of the wavelength of the scattered light. Such dependence could also indicate on scattering particle anisotropy and/or polydispersity. Large polydispersity is in any case obvious from the results presented in Figure 7b. Therefore, these results should only be taken qualitatively, but even as such they clearly indicate on the presence of three distinct populations of scattering particles in the studied two samples. This finding nicely conforms to the electrophoretic and also spectroscopic results presented in the previous paragraphs. The results from Figure 7 also clearly indicate that in the case of slowly cooled sample the proportion of population with small particles with respect to the one with the big particles is much smaller. This can be seen from the smaller first decay in $G_2(\tau)$ function for slowly cooled sample in Figure 7a and also from the ratio of the corresponding two peak heights in Figure 7b. What is even more, Figure 7b also reveals that by filtration the population of small particles was isolated in an important proportion, even though the short tail (representing larger particles in small population) is obviously missing in the filtered sample – see the corresponding $D(R_H)$ distribution functions in Figure 7b.

DLS results were complemented by the SAXS results on the same samples that are depicted in Figure 8. The scattering curves in Figure 8a show on very similar situation in both two samples, with slight differences only in the innermost part of the scattering curves (see inset in in Figure 8a). It has to be cleared out, that the size-resolution of SAXS technique is in this case from size of approximately 1 nm to approximately 27 nm while the information about larger particles is hidden in the primary beam and is not accessible by our experiment. Because of this limitation the SAXS results do not reveal the populations of larger particles that were detected with DLS and other techniques, but can only observe the population of smaller particles. As SAXS is a direct structural method it gives direct structural information on the population of these smaller particles. The most detailed information about the structural features of this population are given via the results of the IFT method presented in Figure 8b. Interestingly the IFT results for filtered and original slowly cooled sample are very similar, both indicating slightly elongated scattering particles with diameter of cross-section of about 3 nm and maximum dimension of 6.5 nm (slight differences in these curves might arise from the difference of the average electron density of these samples and consequent slight difference in the scattering contrast of the scattering particles in these samples). These particles also

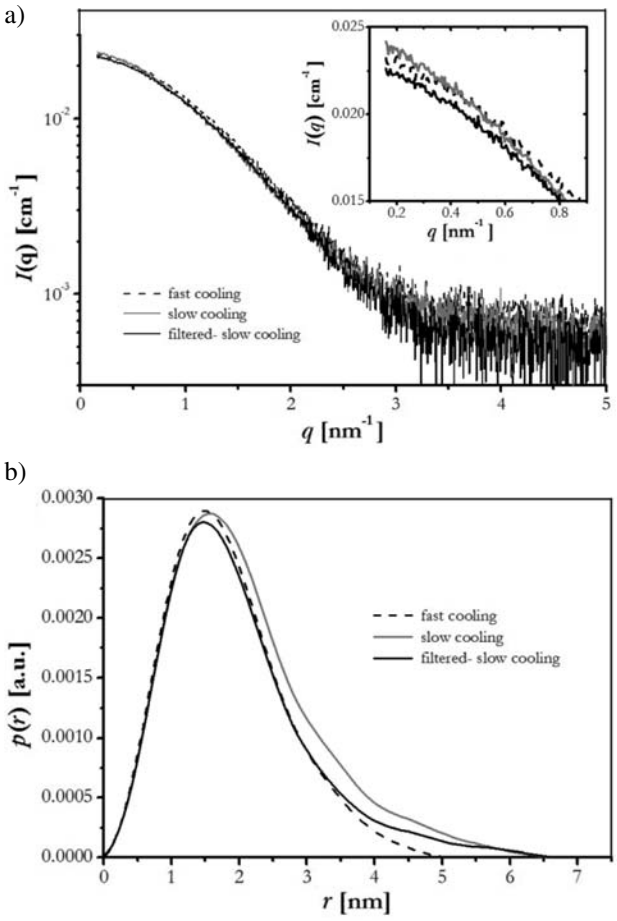

Figure 8. (a) Experimental SAXS curves on absolute scale at 25 °C for the sample with quadruplexes prepared at the cooling rate of either 0.05 °C/min (slow cooling) of the cooling rate of 1 °C/min (fast cooling). The former sample was also filtered through the filter with pore-size of 20 nm. Inset: zoom of the low q part of the scattering curves. (b) Results of the IFT analysis of the SAXS curves: pair-distance distribution functions $p(r)$.

resemble those of fast cooled sample, which seem to be a bit more globular with maximum dimensions of about 5 nm. These results also nicely conform to the values of the hydrodynamic radii obtained for the fastest population of particles in the DLS results.

4. Conclusions

We have used a number of techniques such as UV and CD spectroscopy, DSC, gel electrophoresis, SAXS and DLS to follow thermally induced structure transitions of supermolecular assemblies using a simple 10 nucleotide sequence d($G_4T_2G_4$) in Na^+ solution. Our results show that the formation of investigated assemblies is not a straightforward process but rather involves multiple steps with several structures being formed. We interpreted our data through simultaneous presence of bimolecular and

tetramolecular G-quadruplexes along with G-wires of different lengths, which is in accordance with the suggested conformations that $d(G_4T_2G_4)$ oligonucleotide may adopt (Figure 1). Also all of the experimental techniques showed that thermally induced folding transitions in solution depend on cooling rate and DSC showed that thermally induced unfolding transition depend on heating rate, thus leading to the conclusion that folding/unfolding transitions of structures formed by $d(G_4T_2G_4)$ are kinetically governed processes.

5. Acknowledgement

We acknowledge the financial support of the Slovenian Research Agency through the Physical Chemistry Program Group P1-0201. We would also like to thank prof. dr. Jurij Lah for all his help and support during interpretation of our data.

6. References

1. E. Henderson, C. C. Hardin, S. K. Walk, I. Tinoco, Jr., E. H. Blackburn, *Cell* **1987**, *51*, 899–908.
2. W. I. Sundquist, A. Klug, *Nature* **1989**, *342*, 825–829.
3. E. H. Blackburn, *Cell* **1994**, *77*, 621–623.
4. J. L. Mergny, C. Helene, *Nat Med* **1998**, *4*, 1366–1367.
5. G. N. Parkinson, M. P. Lee, S. Neidle, *Nature* **2002**, *417*, 876–880.
6. H. J. Lipps, D. Rhodes, *Trends Cell Biol* **2009**, *19*, 414–422.
7. A. J. Zaug, E. R. Podell, T. R. Cech, *Proc Natl Acad Sci U S A* **2005**, *102*, 10864–10869.
8. A. M. Zahler, J. R. Williamson, T. R. Cech, D. M. Prescott, *Nature* **1991**, *350*, 718–720.
9. L. H. Hurley, *Nat Rev Cancer* **2002**, *2*, 188–200.
10. P. J. Bates, J. B. Kahlon, S. D. Thomas, J. O. Trent, D. M. Miller, *J Biol Chem* **1999**, *274*, 26369–26377.
11. V. Dapic, P. J. Bates, J. O. Trent, A. Rodger, S. D. Thomas, D. M. Miller, *Biochemistry* **2002**, *41*, 3676–3685.
12. T. Kuwasaki, M. Hatta, H. Takeuchi, H. Takaku, *J Antimicrob Chemother* **2003**, *51*, 813–819.
13. R. F. Rando, J. Ojwang, A. Elbaggari, G. R. Reyes, R. Tinder, M. S. McGrath, M. E. Hogan, *J Biol Chem* **1995**, *270*, 1754–1760.
14. H. Ueyama, M. Takagi, S. Takenaka, *J Am Chem Soc* **2002**, *124*, 14286–14287.
15. T. Simonsson, P. Pecinka, M. Kubista, *Nucleic Acids Res* **1998**, *26*, 1167–1172.
16. A. Siddiqui-Jain, C. L. Grand, D. J. Bearss, L. H. Hurley, *Proc Natl Acad Sci U S A* **2002**, *99*, 11593–11598.
17. M. A. Keniry, *Biopolymers* **2000**, *56*, 123–146.
18. M. Gellert, M. N. Lipsett, D. R. Davies, *Proc Natl Acad Sci U S A* **1962**, *48*, 2013–2018.
19. M. Kaushik, S. Kaushik, A. Bansal, S. Saxena, S. Kukreti, *Curr Mol Med* **2011**, *11*, 744–769.
20. S. Burge, G. N. Parkinson, P. Hazel, A. K. Todd, S. Neidle, *Nucleic Acids Res* **2006**, *34*, 5402–5415.
21. T. I. Gaynutdinov, R. D. Neumann, I. G. Panyutin, *Nucleic Acids Res* **2008**, *36*, 4079–4087.
22. A. T. Phan, V. Kuryavyi, K. N. Luu, D. J. Patel, *Nucleic Acids Res* **2007**, *35*, 6517–6525.
23. T. C. Marsh, E. Henderson, *Biochemistry* **1994**, *33*, 10718–10724.
24. E. Protozanova, R. B. Macgregor, Jr., *Biochemistry* **1996**, *35*, 16638–16645.
25. M. Biyani, K. Nishigaki, *Gene* **2005**, *364*, 130–138.
26. D. Miyoshi, H. Karimata, Z. M. Wang, K. Koumoto, N. Sugimoto, *J Am Chem Soc* **2007**, *129*, 5919–5925.
27. A. N. Lane, J. B. Chaires, R. D. Gray, J. O. Trent, *Nucleic Acids Res* **2008**, *36*, 5482–5515.
28. I. Prislan, J. Lah, G. Vesnaver, *J Am Chem Soc* **2008**, *130*, 14161–14169.
29. I. Prislan, J. Lah, M. Milanic, G. Vesnaver, *Nucleic Acids Res* **2011**, *39*, 1933–1942.
30. T. C. Marsh, J. Vesenka, E. Henderson, *Nucleic Acids Res* **1995**, *23*, 696–700.
31. T. Giorgi, S. Lena, P. Mariani, M. A. Cremonini, S. Masiero, S. Pieraccini, J. P. Rabe, P. Samori, G. P. Spada, G. Gottarelli, *J Am Chem Soc* **2003**, *125*, 14741–14749.
32. M. Bolten, M. Niermann, W. Eimer, *Biochemistry* **1999**, *38*, 12416–12423.
33. A. Wong, R. Ida, L. Spindler, G. Wu, *J Am Chem Soc* **2005**, *127*, 6990–6998.
34. C. R. Cantor, P. R. Schimmel *The behavior of biological macromolecules*; W. H. Freeman: San Francisco, 1980.
35. O. Kratky, H. Stabinger, *Colloid and Polymer Science* **1984**, *262*, 345–360.
36. D. Orthaber, A. Bergmann, O. Glatter, *Journal of Applied Crystallography* **2000**, *33*, 218–225.
37. O. Glatter, in: O. Glatter, O. Kratky (Eds.): Small angle x-ray scattering, Academic Press Inc. London Ltd., London, **1983**, pp. 119–165.
38. O. Glatter, *Journal of Applied Crystallography* **1979**, *12*, 166–175.
39. B. Weyerich, J. Brunner-Popela, O. Glatter, *Journal of Applied Crystallography* **1999**, *32*, 197–209.
40. J. Brunner-Popela, O. Glatter, *Journal of Chemical Physics* **1999**, *110*, 10623–10632.
41. G. Fritz, A. Bergmann, O. Glatter, *Journal of Chemical Physics* **2000**, *113*, 9733–9740.
42. O. Glatter, in: P. Lindner, T. Zemb (Eds.): Neutron, X-rays and Light: Scattering Methods Applied to Soft Condensed Matter, Elsevier, Amsterdam, **2002**.
43. G. Fritz, O. Glatter, *Journal of Physics – Condensed Matter* **2006**, *18*, S2403–S2419.
44. O. Glatter, *Acta Physica Austriaca* **1977**, *47*, 83–102.
45. O. Glatter, *Journal of Applied Crystallography* **1977**, *10*, 415–421.
46. O. Glatter, *Journal of Applied Crystallography* **1980**, *13*, 577–584.
47. O. Glatter, in: O. Glatter, O. Kratky (Eds.): Small Angle X-

Ray Scattering, Academic Press Inc. London Ltd., London, **1983**, pp. 167–196.
48. M. Smoluchowski, *Annalen der Physik* **1908**, *330*, 205–266.
49. A. Einstein, *Annalen der Physik* **1910**, *338*, 1275–1298.
50. P. N. Pusey, R. J. A. Tough *Dynamic Light scattering. Applications of Photon Correlation Spectroscopy*; Plenum: New York, 1985.
51. J. Langowsky, R. Brian *Neutron, X-Ray and Light Scattering*; North Holland: Amsterdam, **1991**.
52. A. J. F. Siegert, *MIT radiation laboratory report* **1943**, *465*.
53. H. Schnablegger, O. Glatter, *Applied Optics* **1991**, *30*, 4889–4896.
54. J. Kypr, I. Kejnovska, D. Renciuk, M. Vorlickova, *Nucleic Acids Res* **2009**, *37*, 1713–1725.
55. M. Vorlickova, J. Chladkova, I. Kejnovska, M. Fialova, J. Kypr, *Nucleic Acids Res* **2005**, *33*, 5851–5860.
56. I. N. Rujan, J. C. Meleney, P. H. Bolton, *Nucleic Acids Res* **2005**, *33*, 2022–2031.
57. L. Spindler, M. Rigler, I. Drevensek-Olenik, N. Ma'ani Hessari, M. Webba da Silva, *J Nucleic Acids* **2010**, *2010*.

Povzetek

DNA najpogosteje obravnavamo kot dvoverižno molekulo, v kateri sta dva komplementarna niza med seboj povezana z Watson-Crick-ovimi baznimi pari. Z gvanini bogata zaporedja DNA pa lahko tvorijo tudi drugačne, bolj nenavadne strukture, ki so sestavljene iz t.i. G-kvartetov. Možnost uporabe v molekularni elektroniki je zbudila zanimanje za samoureje nenanostrukture, ki so jih poimenovali G-žičke. Zadali smo si cilj, da bi bolje razumeli strukturne prehode G-žičk, ki nastanejo iz oligonukleotida d($G_4T_2G_4$). V ta namen smo uporabili vrsto eksperimentalnih tehnik; UV in CD spektroskopijo, diferen no dinami no kalorimetrijo (DSC), gelsko elektroforezo, ozkokotno rentgensko sipanje (SAXS) in dinami no sipanje svetlobe (DLS).. Vse eksperimentalne tehnike so pokazale, da sta nastanek in ureditev struktur odvisna od hitrosti ohlajanja, DSC pa je pokazala, da je razvijanje struktur odvisno od hitrost gretja. To nas je pripeljalo do zaključka, da sta tvorba in razvitje struktur, ki nastanejo iz oligonukleotida d($G_4T_2G_4$), kinetično pogojena.